Nano Energy 35 (2017) 92–100

Contents lists available at ScienceDirect

Nano Energy

journal homepage: www.elsevier.com/locate/nanoen

Full paper

Manipulation of charge transfer in vertically aligned epitaxial ferroelectric $KNbO_3$ nanowire array photoelectrodes

Shun Li[a,1], Jianming Zhang[b,1], Bo-Ping Zhang[a,*], Wei Huang[c], Catalin Harnagea[c], Riad Nechache[d], Lifeng Zhu[a], Suwei Zhang[a], Yuan-Hua Lin[e,*], Liang Ni[b], Yuan-Hua Sang[f], Hong Liu[f], Federico Rosei[c,*]

[a] School of Materials Science and Engineering, University of Science and Technology Beijing, Beijing 100083, China
[b] School of Chemistry and Chemical Engineering, Jiangsu University, Zhenjiang 212013, China
[c] Institut National de la Recherche Scientifique, Centre Énergie, Matériaux et Télécommunications, 1650, Boulevard Lionel-Boulet, Varennes, Québec, Canada J3X 1S2
[d] Department of Electrical Engineering, École de Technologie Supérieure, 1100 Notre-Dame Ouest, Montréal, Québec, Canada H3C 1K3
[e] School of Materials Science and Engineering, Tsinghua University, Beijing 100084, China
[f] State Key Laboratory of Crystal Materials, Shandong University, Jinan 250100, China

ARTICLE INFO

Keywords:
Epitaxial
$KNbO_3$ nanowire array
Photoelectrochemistry
Ferroelectric polarization

ABSTRACT

We demonstrate the growth and characterization of an array of ferroelectric nanowires for photoelectrochemical (PEC) hydrogen production. The photoelectrodes are made of vertically aligned one-dimensional nanowires of the "classic" ferroelectric perovskite $KNbO_3$ grown epitaxially on a Nb-doped $SrTiO_3$ substrate. The charge transfer properties of the photoelectrodes can be effectively tuned by controlling the polarization state, thereby optimizing PEC performance. By manipulating the poling bias from +15 V to −15 V, we were able to tune the photocurrent density in the range from ca. 0.7–11.5 $\mu A \cdot cm^{-2}$ (at 0 V vs. Ag/AgCl) under irradiation of air mass 1.5 global (AM 1.5 G) full sunlight at 100 mW/cm^2, while the onset potential switches from −0.32 to −0.46 V. Our work provides the basis for understanding PEC reactions conducted with ferroelectric nanowire photoelectrodes as well as insights on strategies for constructing high performance nanowire array-based PEC systems.

1. Introduction

The growing global demand for renewable and sustainable energy has prompted major efforts towards developing new solar technologies. In particular, harnessing solar energy for hydrogen production by using a photoelectrochemical (PEC) cell represents a very attractive approach towards alternative clean fuels [1–4].

Major research efforts have focused on developing materials usable as photoelectrodes, which are a key component in a PEC cell. Among various challenges, the performance of conventional photoelectrode materials (n-type TiO_2 [5], ZnO [6], α-Fe_2O_3 [7], $BiVO_4$ [8,9] and WO_3 [10,11]; p-type Si [12,13], Cu_2O [14] and $CaFe_2O_4$ [15], *etc.*) is still limited by their relatively low absorption coefficient, short carrier diffusion length, and the fast recombination rate of photogenerated charge carriers. Current strategies to optimize the separation of electron-hole pairs in photoelectrodes mainly focus on chemical and structural optimization (e.g. control of morphology and crystallography), which are limited by the synthesis techniques currently in use.

An alternative approach to overcome the limitations of conventional semiconductors is to fabricate photoelectrodes made of ferroelectric materials [16–18]. The key advantage of ferroelectric systems is associated with their remnant polarization, which creates a depolarization electric field (E_{dp}) that extends over the entire volume of the film or bulk material. This field may replace the electrical field that forms in a classical p-n junction, effectively separating electron-hole pairs and driving them towards electrodes; this phenomenon is generally referred to as the ferroelectric photovoltaic effect (FPVE) [19–22]. This internal electrical field also gives rise to the modulation of the chemical potential and surface band bending, which are the essential factors that determine PEC performance [23]. Recent studies reported several ferroelectric photoelectrodes such as $LiNbO_3$ [24], $BaTiO_3$ [25–27], $Pb(Zr,Ti)O_3$ (PZT) [28,29], $BiFeO_3$ [30–32] and Bi_2FeCrO_6 [33] with large and reversible polarization, showing an enhanced PEC activity by controlling the ferroelectric polarization.

* Corresponding authors.
E-mail addresses: bpzhang@ustb.edu.cn (B.-P. Zhang), linyh@tsinghua.edu.cn (Y.-H. Lin), rosei@emt.inrs.ca (F. Rosei).
[1] These authors contributed equally to this work.

http://dx.doi.org/10.1016/j.nanoen.2017.03.033
Received 6 February 2017; Received in revised form 15 March 2017; Accepted 16 March 2017
Available online 18 March 2017

While extensive research has focused on semiconductor/electrolyte interfaces with planar geometry, recent advances in nanofabrication enabled the use of nanostructured semiconductors for PEC hydrogen production [3,34–36]. Among various categories of nanomaterials, vertically aligned arrays of semiconductor nanowires (NWs) are of particular interest because of their large semiconductor/electrolyte interfacial areas in addition to other beneficial properties, including enhanced light scattering and trapping, and efficient ballistic charge transport along the wire's axis [37–40]. As a result, devices based on NW arrays are promising towards the wide scale adoption of solar technologies based on low cost-to-power requirements.

Several studies reported various planar ferroelectric photoelectrodes [28,30,31,41–43], yet far less information is available regarding devices for solar hydrogen production based on arrays of ferroelectric NWs. For example, PEC activity enhanced by ferroelectric polarization was observed for a $TiO_2/BaTiO_3$ core/shell NW photoanode [44]. These studies motivated us to develop photoelectrodes made of ferroelectric NW arrays, to take full advantage of their unique electrical and optical properties.

Potassium niobate ($KNbO_3$, KNO), a classic perovskite oxide with intriguing ferroelectric properties, suitable band positioning, excellent chemical stability, as well as non-toxicity compared to lead-based materials such as PZT, has been used successfully in various photocatalytic processes, including hydrogen production [45–48], degradation of organic pollutants [49–51], and CO_2 conversion [52]. In particular, Park *et al*. reported that polarized $K_{0.5}Na_{0.5}NbO_3$ powder exhibits a significantly enhanced photocatalytic activity (ca. 7 fold), compared to that of the neutral sample [53].

Inspired by these studies, herein we chose KNO as a model system to explore the role of the polarization state in the PEC behavior of photoelectrodes made of arrays of ferroelectric NWs. We demonstrate that the internal field induced by the polarization of KNO NWs can effectively tune the charge transfer characteristics of photo-excited electron-hole pairs.

2. Experimental

2.1. Synthesis of $KNbO_3$ nanowire arrays

Arrays of single-crystalline KNO NWs were epitaxially grown on Nb-doped (0.7 wt%) $SrTiO_3$ (NSTO) (100) by a hydrothermal method [54]. NSTO was chosen as substrate because of its electrical conductivity. The substrate was cleaned by sonication in acetone, ethanol and deionized water, respectively. In a typical reaction, an alkaline aqueous solution was obtained by dissolving 6.312 g of potassium hydroxide (KOH) in 7.5 mL of deionized water. Subsequently, 0.437 g of niobium (Nb) metal powder was added to the solution. The suspension was then transferred to a Teflon-lined autoclave (20 mL), in which the cleaned NSTO substrate was positioned face down and placed ca. 1 cm above the bottom of the Teflon liner. The autoclave was kept in an oven at 150 °C for 12 h. After cooling down to room temperature, the sample was rinsed with deionized water and dried at 60 °C.

2.2. Characterizations

X-ray diffraction (XRD) was used to analyze the crystal structure using a high resolution Panalytical X'pert Pro diffractometer. To investigate crystal orientation, we carried out ϕ-scans by 360° in-plane sample rotation around the (101) plane of the NSTO substrate. Characterization of sample morphology and chemical composition were performed by field-emission scanning electron microscopy (FESEM) (JEOL JSM7401F) equipped with an energy-dispersive X-ray spectrometer (EDX). Transmission electron microscopy (TEM) and selected area electron diffraction (SAED) images were obtained using a FEI Tecnai G2 F20 microscope. Diffuse reflectance spectra (DRS) were recorded by UV–visible spectroscopy (Hitachi U-3010) with an integration sphere. Piezoresponse force microscopy (PFM) measurements were performed using a Veeco Enviroscope atomic force microscope (AFM) equipped with Pt/Ir coated ANSCM-PA probes from App Nano with cantilever spring constant of ~40 N/m (resonance frequency ~300 kHz). We applied an AC voltage of 0.5 V at 26 kHz between the conductive tip and the NSTO conductive substrate. The bias required for hysteresis measurements was applied using a DC source (Keithley 2400 Sourcemeter) in series with an AC driving voltage. Macroscopic ferroelectric hysteresis loop of the sample was obtained using a ferroelectric tester (Radiant Technologies RT6000HVA) at a frequency of 100 Hz. The voltage was directly applied between the NSTO bottom electrode and the top of KNO NW arrays without depositing a top electrode.

2.3. Photoelectrochemical measurements

All PEC measurements were performed on an electrochemical workstation (Chenhua CHI 660D) in a three-electrode system using the KNO NW array photoanodes as the working electrode, a Pt plate as the counter electrode, and a standard Ag/AgCl electrode as reference. A 300 W xenon lamp equipped with an AM1.5 filter was used as irradiation source with a light intensity of 100 mW/cm^2 measured with a radiometer. 1 M Na_2SO_4 aqueous solution was employed as electrolyte. The linear sweep voltammograms were carried out at a scan rate of 20 mV/s. Photocurrent density measurements as a function of time (*J-t*) of the photoanodes with on and off cycles were carried out at a fixed bias of 0 V *vs*. Ag/AgCl. Electrochemical impedance spectroscopy (EIS) measurements were conducted with an amplitude of 5 mV over a frequency ranging from 0.01 to 100 kHz. Poling of the NW arrays was performed in 2 M KCl aqueous solution using Pt as counter electrode by applying a bias with a DC power supply for 60 s. The experimental setup for the poling treatment is schematically shown in Fig. S1 in the Supporting information file.

3. Results and discussion

The synthesis of vertically aligned KNO NW arrays is based on a simple hydrothermal reaction without seed layer. Fig. 1a and b show tilt-view SEM images of the as-grown KNO NW arrays on NSTO substrate. The NWs are vertically aligned, with width ranging from 100 to 200 nm and a height of ca. 8 μm. The NWs are asymmetric, resembling a stepped structure, demonstrating an anisotropic growth of the wires (see enlarged SEM image in Fig. S2a). At the initial growth stage, a thick film with thickness of ca. 2 μm was formed on the NSTO substrate by nucleation and coalescence of square islands, as observed from the top view in Fig. S2b, consistent with previous reports [55]. The width of the islands shrinks along the growth direction. The islands develop into tower-like structures, suggesting a dislocation-assisted growth mechanism [56]. EDX measurements were carried out to evaluate the chemical composition of the NW arrays (Fig. S2c), indicating that the wires consist of K, Nb and O.

The out-of-plane orientation and phase purity of the sample were investigated by high-resolution XRD θ–2θ scans. The as-grown NW arrays (Fig. 2a) exhibit three sets of mixed $(ll0)_o/(00\ l)_{pc}$ orientation, as inferred by the presence of (110)/(001), (220)/(002) and (330)/(003) diffraction peaks. The diffraction peaks only indicative of $SrTiO_3$ or $KNbO_3$ phases were detected, suggesting that the NW arrays are *c*-oriented with a single phase perovskite structure.

To further establish the in-plane epitaxial relationship between the NW arrays and the substrate, we acquired XRD ϕ scans on the (101) diffraction peaks of the NWs and substrate. Only four peaks separated from each other by 90° were found at the same position for both the KNO and NSTO (Fig. 2d), revealing that the epitaxial relationship between the NW arrays and the substrate has a fourfold symmetry: KNO $[001]_{pc}$//NSTO $[001]_c$. The appearance of both (110) and (001) orientations is attributed to the significantly reduced difference in

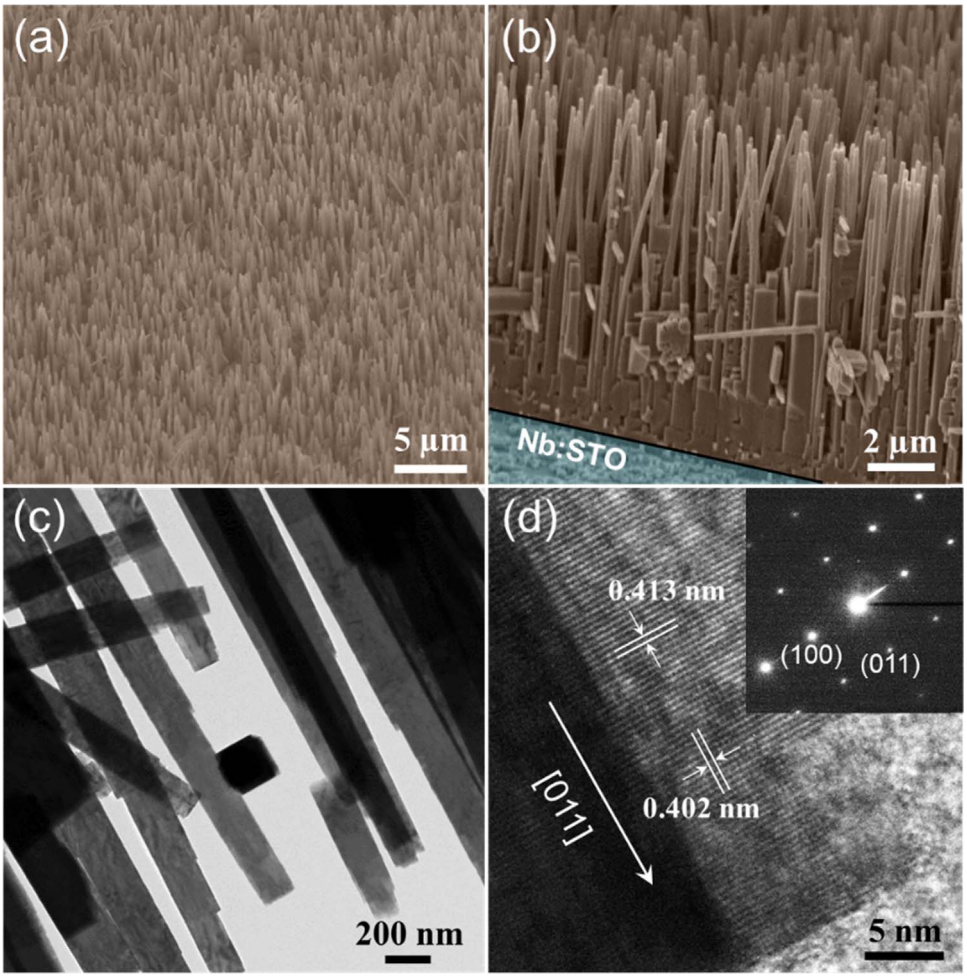

Fig. 1. (a, b) SEM images of KNO NW arrays epitaxially grown on NSTO (100) substrate. (c) Low-magnification TEM and (d) HR-TEM image of the KNO NWs. SAED patterns are shown in the inset of (d).

lattice mismatch seen by each orientation, resulting from the anisotropic lattice expansion [56].

The sample's crystal structure was further investigated by high-resolution transmission electron microscopy (HR-TEM). As shown in Fig. 1d, an individual NW shows pseudocubic lattice parameters in the orthorhombic phase of the (100) and (011) planes with lattice spacings of a=4.02 Å and c=4.13 Å, respectively. The SAED pattern (inset of Fig. 1d) is well-defined, indicating that the NWs are single crystals. Based on these results, we conclude that the KNO NWs grow along the [011] direction. Consistent with previous reports [55,57], both TEM and XRD characterizations confirm that the KNO NW arrays grown on NSTO exhibit a stable orthorhombic phase, instead of a metastable monoclinic phase. We consider that the epitaxial strain from the NSTO substrate (cubic) may stabilize the more symmetric orthorhombic structure during synthesis [55], rather than the monoclinic one. The spontaneous polarization of KNO is along the [001] direction [57], which is 45° off the long axis of the NW.

The local piezoelectric/ferroelectric characteristics of individual vertically aligned KNO NWs were assessed by measuring the piezoelectric response phase and amplitude under an applied DC bias. The experimental setup is schematically illustrated in Fig. 3a. Fig. 3b displays an AFM topographic image of the NW arrays, acquired in noncontact mode at low scan speed. As shown in Fig. 3c, amplitude butterfly loops were observed, along with abrupt phase changes from 90° to −90° when sweeping the DC voltage, demonstrating local switching of ferroelectric polarization in the NWs. The corresponding piezoelectric response as a function of applied voltage shows a hysteretic behavior (Fig. 3d). The hysteresis loops exhibit a highly asymmetric shape (saturated at 0 V), which indicates the existence of a spontaneous polarization (P_s) in the KNO NWs. The direction of P_s points 45° up from the substrate towards the top of the NW. We repeated PFM measurements on several randomly selected NWs, obtaining similar/consistent results.

A key question for such systems is to determine whether one-dimensional wires exhibit any spontaneous ferroelectric ordering. Theoretical work predicted quantitatively that a large spontaneous polarization of the bulk magnitude exists in one dimensional Pb(ZrTi)O_3 wires [58]. Herein, surprisingly, our experimental results demonstrate the existence of a strong spontaneous polarization in the as-grown KNO NWs by a facile chemical route. To understand the ferroelectric behavior of the NW arrays at the macroscale, we further measured ferroelectric hysteresis loops of the whole sample, as illustrated in Fig. S3a. The remnant polarization is about 90 μC/cm^2 (Fig. S3b), much higher than that of epitaxial KNO thin films [59,60]. Further theoretical and experimental studies are needed to understand the origin of such strong spontaneous polarization in the as-prepared KNO ferroelectric NWs. The distinct ferroelectric performance of the obtained KNO NW arrays allows us to manipulate the internal electric field induced by polarization and thus to tune the charge transfer behavior in NW based photoelectrodes.

Before investigating the hydrogen production performance of the KNO NWs, we characterized their photoabsorption properties. The UV–vis diffuse reflectance spectrum (Fig. 4b) of the as-prepared sample was measured and converted into absorption readings accord-

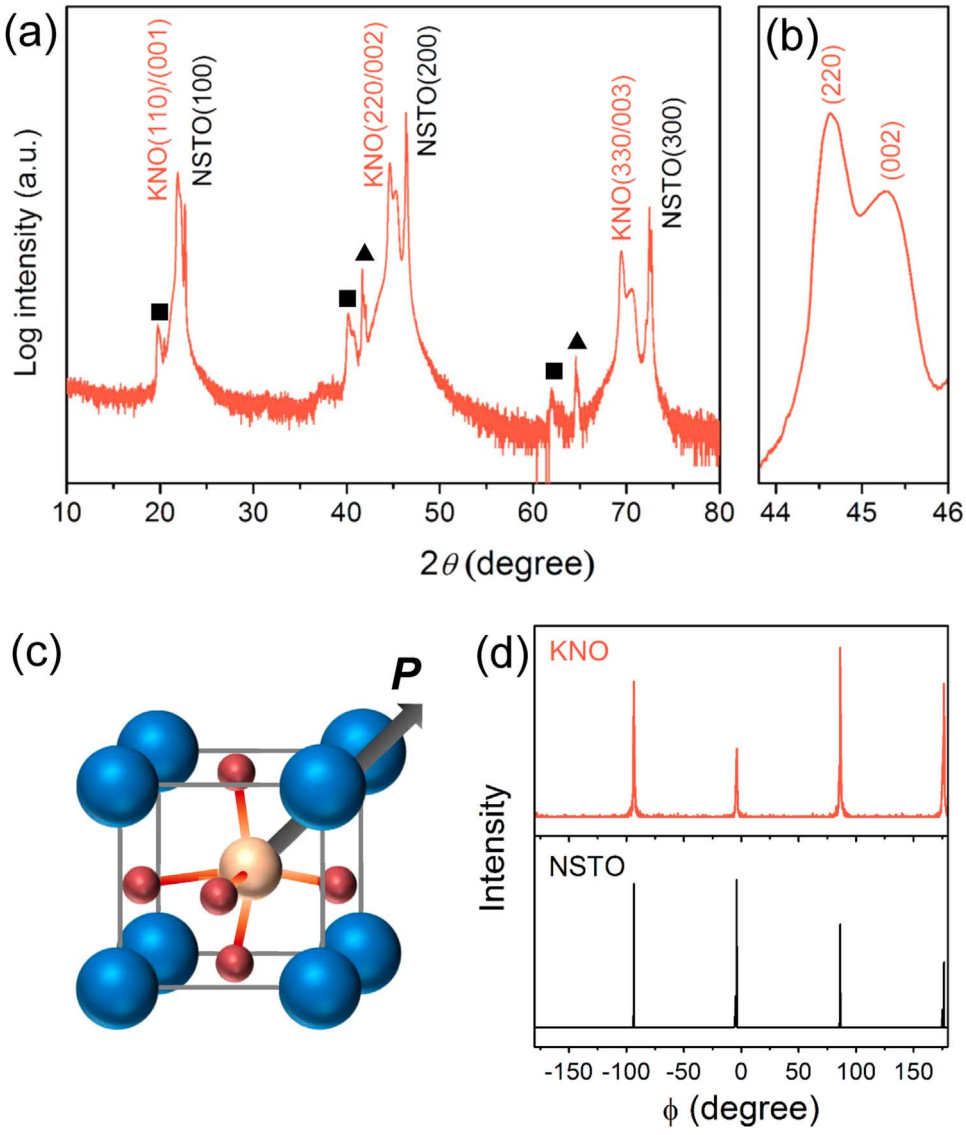

Fig. 2. (a) XRD patterns of the as-grown KNO NW arrays on a NSTO (100) substrate. The squares in the figure correspond to K_β peaks, while the triangles indicate tungsten contamination from the X-ray tube cathode. (b) A magnified view of the selected-range XRD patterns. (c) Crystal structure of KNO unit cell. The black arrow indicates one of the possible directions of the electric polarization *P*. (d) Corresponding 360° ϕ-scan measurements around the (101) plane of the NSTO substrate.

ing to the Kubelka-Munk (K-M) method [61]. The absorption spectrum shows a sharp optical band transition at ca. 380 nm, with an estimated band gap (E_g) of ~3.28 eV (inset of Fig. 4b). The E_g is close to the reported value for orthorhombic KNO nanocubes (3.2 eV), and somewhat wider than that of KNO microcubes (3.15 eV) [47]. The difference is attributed to size effects of the NWs. In contrast to a powdered KNO sample which typically appears white due to its wide band gap [54], KNO NW arrays appear as dark grey, as shown by the digital image in the inset of Fig. 4b. This is evidenced by the appearance of the absorption tail in longer wavelengths, which could be ascribed to the strong light scattering of the NWs [62].

Polarization engineering in ferroelectrics is crucial to tune the depolarization (internal) electric field and obtain optimal surface band structures to enhance their PEC properties. Herein, we aim to understand the polarization controlled PEC performance and charge transfer behavior in ferroelectric NWs.

KNO NW arrays used as photoanode are presented in Fig. 4a. Fig. 4c displays representative linear sweep voltammetry (*J-V*) curves for the KNO/NSTO photoelectrodes, as well as the sample that has undergone poling pretreatments with two different directions (± 15 V). We poled the photoelectrodes in 2 M KCl solution by applying a DC bias, as reported previously [44]. All PEC measurements were conducted in an electrolyte consisting of 1 M Na_2SO_4 aqueous solution under AM 1.5 G (100 mW/cm^2) simulated sunlight irradiation. For comparison purposes, the top axis was converted to the reversible hydrogen electrode (RHE) scale using the following expression $E_{RHE}=E_{Ag/AgCl}+0.0591$ V pH +0.197 V.

Under simulated solar irradiation (Fig. 4c, upper panel), a net photocurrent density (J_{ph}) of ca. 1.5 μA cm^{-2} was observed for the as-grown NWs array sample at the thermodynamic potential (+0.62 V *vs.* Ag/AgCl). The sample poled with +15 V (middle of Fig. 4c) exhibited a very similar J_{ph} (1.2 μA cm^{-2}), implying that the spontaneous polarizations in the as-grown single crystalline KNO NWs are highly aligned and optimized along this direction. This is consistent with PFM analysis. By contrast, after negative (−15 V) poling (lower panel of Fig. 4c), the J_{ph} drastically increased to ca. 21.8 μA cm^{-2} at the same bias. The onset potential switches from −0.32 V to −0.46 V when the poling bias of pretreatment switched from +15 V to −15 V, which is favorable for decomposing water with the KNO photoanode.

To examine the instant photoresponse for the electrodes, we

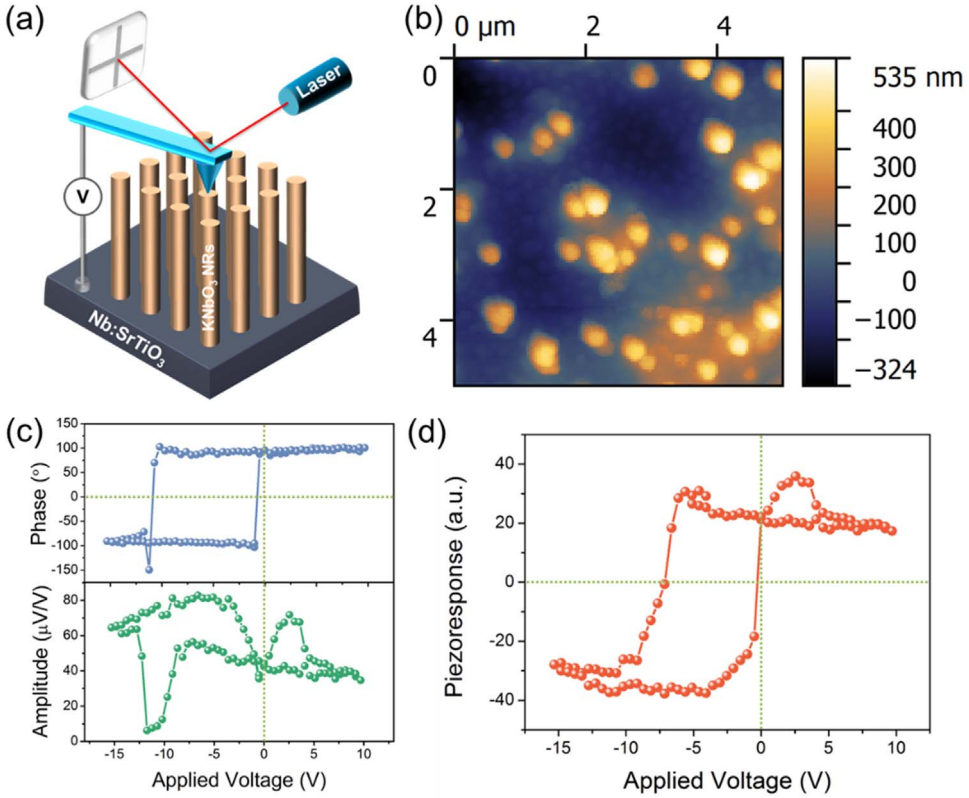

Fig. 3. (a) Schematic illustration of PFM measurement on a single KNO NW. (b) AFM topography image showing the surface of the NW arrays. DC bias induced local PFM (c) phase signal and piezoelectric strain amplitude, and (d) piezoresponse curve of a single KNO NW.

collected chronoamperometric *J-t* curves under chopped light illumination at 0 V versus Ag/AgCl. As shown in Fig. 4d, the recorded photocurrent densities are consistent with the values obtained from the linear sweep voltammagrams. After poling with −15 V, the J_{ph} enhanced to 11.5 μA cm^{-2} (at 0 V *vs*. Ag/AgCl) under illumination, more than 10-fold larger than that of the same sample that underwent +15 V poling (0.7 μA cm^{-2}). These values show that the performance of the KNO NW array based photoelectrodes can be effectively tuned.

To understand the effect of polarization in greater depth, we carried out PEC measurements on samples poled with lower voltages (± 5 V). As expected, the J_{ph} remained practically unchanged after poling with +5 V bias, while slightly increased to ca. 1.1 μA cm^{-2} at zero bias following a −5 V poling treatment. This indicates that the voltage applied is not sufficient to switch a significant number of ferroelectric domains in the KNO NWs. To rule out other factors, we performed the same set of poling treatments and PEC measurements for similar NW array photoanodes made of TiO_2 (a non-ferroelectric oxide). The results showed that the electric poling barely affected its performance. These results clearly demonstrate that the increase of photocurrent in the KNO NW based photoanode after poling originates only from modification of ferroelectric polarization in the NWs.

To further understand the PEC water oxidation behavior, we measured the electrochemical impedance spectrum (EIS), which is an effective method for appraising the intrinsic charge-transfer resistance. As shown in Fig. 4e, the negatively (−15 V) poled KNO NW electrode shows a much smaller arc radius in the EIS than that of the positively (+15 V) poled sample, suggesting its faster interface charge transport. Therefore, EIS results indicate an enhanced separation of photoexcited charge carriers in negatively poled NWs, which is beneficial to the PEC performance of the KNO photoanode.

On the basis of the aforementioned analysis, it is desirable to regulate the polarization state (internal electric field) and migration of photogenerated holes, so as to obtain high-efficiency oxygen-evolving ferroelectric KNO NW based photoanodes. The proposed mechanism could be explained as follows. An upward poling (P_{up}) results in an E_{dp} (opposite to the polarization direction) which drives the positive charges accumulated on the NW's surface and negative ones to the bottom electrode (Fig. 5a), while downward poled (P_{down}) KNO NWs lead to an opposite E_{dp} (Fig. 5b). Fig. 5c and d display schematic band structures of the NSTO/KNO/electrolyte heterojunction for the two poling directions. The Fermi level position of NSTO is at −0.4 eV *vs*. NHE [21], and the conduction band minimum (CBM) and valence band maximum (VBM) position of KNO is at −0.78 eV and 2.36 eV, respectively [63].

For a positively poled sample (Fig. 5c), the photogenerated electrons and holes could be easily trapped in the KNO NW photoanode due to the downward band bending at the KNO/electrolyte junction and upward bending near the NSTO/KNO junction. This would prevent photogenerated holes from moving to the surface of the KNO NWs, as well as the transfer of electrons to the NSTO bottom electrode. On the other hand, the negative pretreatment potential switches the internal field so that it points towards the top of the KNO NW and yields an opposite band bending at both junctions (Fig. 5d), compared to the sample poled positively. Due to the favorable band bending, the photogenerated e^-/h^+ pairs in the KNO NWs will be separated effectively by the driving force arising from E_{dp} created by the polarization; the electrons will move toward the NSTO substrate, while the holes will migrate to the electrolyte, leading to an enhanced PEC activity.

The controllable charge transfer behavior observed in the ferroelectric KNO NWs opens the possibility of designing a complete PEC cell with only ferroelectric electrodes that behave as photoanodes or photocathodes relying on the choice of poling biases. Additionally, such tunable reactions could also be applied to other electrochemical processes. Further investigations are in progress on ferroelectric NWs with narrow band gap to fully use the solar spectrum to improve the PEC performance.

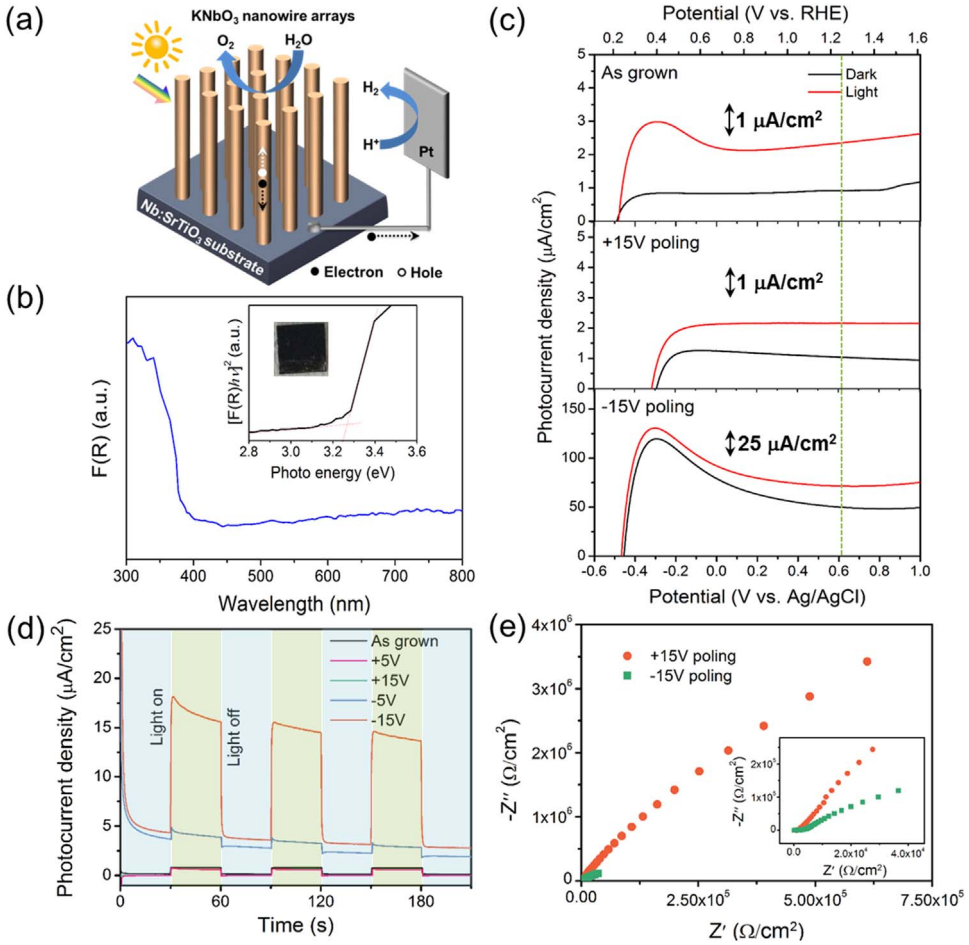

Fig. 4. (a) Schematic illustration of PEC water splitting on KNO NW arrays. (b) UV–vis diffuse reflectance spectra of the as-grown KNO NW arrays. Inset: calculation of band gap energy by Tauc equation and photograph of 10×10 mm^2 sample with low reflection. (c) Linear sweep voltammetry curves and (d) transient photocurrent responses for the as-grown KNO NW array photoelectrode and after poling with two opposite directions under AM 1.5 G simulated sunlight (100 mW/cm^2) at zero bias (0 V *vs.* $V_{Ag/AgCl}$). The thermodynamic potential for water oxidation (1.23 V *vs.* RHE) is noted by the green line. (e) EIS curves with two different ferroelectric polarization directions. Inset shows a magnified view of a selected range.

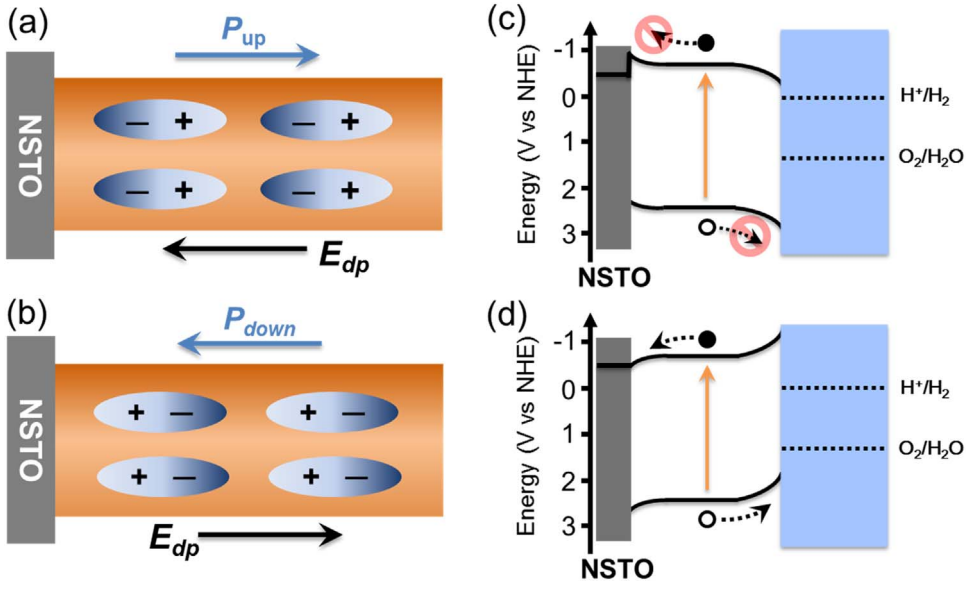

Fig. 5. A schematic diagram showing polarization bound charge under two different oriented polarization conditions: (a) positively and (b) negatively poled KNO NW arrays. *P* is the polarization, and E_{dp} is the depolarization field. (c and d) Proposed electronic band structure and the mechanisms for the charge transfer process in the KNO NW array photoelectrodes for the two poling configurations.

4. Conclusions and perspectives

In summary, we demonstrated tunable PEC properties in vertically aligned epitaxial ferroelectric KNO NW arrays grown by hydrothermal synthesis. Local PFM measurements and macroscopic ferroelectric tests were performed to investigate the piezoelectric/ferroelectric behavior of the KNO NWs along the growth direction, demonstrating ferroelectric long-range order in the wires. As a result of their prominent ferroelectric properties, the KNO NW array photoelectrodes can tune the transport of photogenerated charges by manipulating the built-in potential provided by the ferroelectric domains. The photocurrent and onset potential of the KNO NW photoanode depends substantially on the poling treatments, and the negatively poled sample demonstrated an enhanced PEC performance. This study highlights the potential of ferroelectric or piezoelectric potential-induced band structure engineering for optimizing the performance of ferroelectric NW array photoelectrodes.

Acknowledgements

B.-P.Z. acknowledges the National Natural Science Foundation of China (Grant No. 51272023 and 51472026). F.R. acknowledges infrastructure support from the Canada Foundation for Innovation, NSERC for a discovery grant and partial salary support from the Canada Research Chair in Nanostructured Materials. S.L. thanks the Fundamental Research Funds for the Central Universities (Grant No. FRF-TP-15-076A1), and the China Postdoctoral Science Foundation (Grant No. 2015M580984).

Appendix A. Supporting information

Supplementary data associated with this article can be found in the online version at doi:10.1016/j.nanoen.2017.03.033.

References

[1] T. Hisatomi, J. Kubota, K. Domen, Chem. Soc. Rev. 43 (2014) 7520–7535.
[2] C. Liu, J. Tang, H.M. Chen, B. Liu, P. Yang, Nano Lett. 13 (2013) 2989–2992.
[3] F.E. Osterloh, Chem. Soc. Rev. 42 (2013) 2294–2320.
[4] L. Jin, G. Sirigu, X. Tong, A. Camellini, A. Parisini, G. Nicotra, C. Spinella, H. Zhao, S. Sun, V. Morandi, M. Zavelani-Rossi, F. Rosei, A. Vomiero, Nano Energy 30 (2016) 531–541.
[5] S.U. Khan, M. Al-Shahry, W.B. Ingler, Science 297 (2002) 2243–2245.
[6] C. Zhang, M. Shao, F. Ning, S. Xu, Z. Li, M. Wei, D.G. Evans, X. Duan, Nano Energy 12 (2015) 231–239.
[7] A. Kleiman-Shwarsctein, Y.-S. Hu, A.J. Forman, G.D. Stucky, E.W. McFarland, J. Phys. Chem. C 112 (2008) 15900–15907.
[8] W. Luo, Z. Yang, Z. Li, J. Zhang, J. Liu, Z. Zhao, Z. Wang, S. Yan, T. Yu, Z. Zou, Energ. Environ. Sci. 4 (2011) 4046–4051.
[9] J.-S. Yang, J.-J. Wu, Nano Energy 32 (2017) 232–240.
[10] T.W. Kim, K.-S. Choi, Science 343 (2014) 990–994.
[11] S. Wang, H. Chen, G. Gao, T. Butburee, M. Lyu, S. Thaweesak, J.-H. Yun, A. Du, G. Liu, L. Wang, Nano Energy 24 (2016) 94–102.
[12] Y. Hou, B.L. Abrams, P.C.K. Vesborg, M.E. Björketun, K. Herbst, L. Bech, A.M. Setti, C.D. Damsgaard, T. Pedersen, O. Hansen, J. Rossmeisl, S. Dahl, J.K. Nørskov, I. Chorkendorff, Nat. Mater. 10 (2011) 434–438.
[13] X.-Q. Bao, D.Y. Petrovykh, P. Alpuim, D.G. Stroppa, N. Guldris, H. Fonseca, M. Costa, J. Gaspar, C. Jin, L. Liu, Nano Energy 16 (2015) 130–142.
[14] A. Paracchino, V. Laporte, K. Sivula, M. Grätzel, E. Thimsen, Nat. Mater. 10 (2011) 456–461.
[15] S. Ida, K. Yamada, T. Matsunaga, H. Hagiwara, Y. Matsumoto, T. Ishihara, J. Am. Chem. Soc. 132 (2010) 17343–17345.
[16] L. Li, P.A. Salvador, G.S. Rohrer, Nanoscale 6 (2014) 24–42.
[17] M.A. Khan, M.A. Nadeem, H. Idriss, Surf. Sci. Rep. 71 (2016) 1–31.
[18] D. Tiwari, S. Dunn, J. Mater. Sci. 44 (2009) 5063–5079.
[19] T. Choi, S. Lee, Y.J. Choi, V. Kiryukhin, S.W. Cheong, Science 324 (2009) 63–66.
[20] W. Ji, K. Yao, Y.C. Liang, Adv. Mater. 22 (2010) 1763–1766.
[21] R. Nechache, C. Harnagea, S. Li, L. Cardenas, W. Huang, J. Chakrabartty, F. Rosei, Nat. Photonics 9 (2015) 61–67.
[22] R. Guo, L. You, Y. Zhou, Z.S. Lim, X. Zou, L. Chen, R. Ramesh, J. Wang, Nat. Commun. 4 (2013) 1990.
[23] M.B. Starr, X. Wang, Nano Energy 14 (2015) 296–311.
[24] Y. Inoue, M. Okamura, K. Sato, J. Phys. Chem. 89 (1985) 5184–5187.
[25] Y. Cui, J. Briscoe, S. Dunn, Chem. Mater. 25 (2013) 4215–4223.
[26] H. Li, Y. Sang, S. Chang, X. Huang, Y. Zhang, R. Yang, H. Jiang, H. Liu, Z.L. Wang, Nano Lett. 15 (2015) 2372–2379.
[27] N.V. Burbure, P.A. Salvador, G.S. Rohrer, Chem. Mater. 22 (2010) 5823–5830.
[28] C. Wang, D. Cao, F. Zheng, W. Dong, L. Fang, X. Su, M. Shen, Chem. Commun. 49 (2013) 3769–3771.
[29] Z. Wang, D. Cao, L. Wen, R. Xu, M. Obergfell, Y. Mi, Z. Zhan, N. Nasori, J. Demsar, Y. Lei, Nat. Commun. 7 (2016) 10348.
[30] D. Cao, Z. Wang, Nasori, L. Wen, Y. Mi, Y. Lei, Angew. Chem. Int. Ed. 126 (2014) 11207–11211.
[31] W. Ji, K. Yao, Y.-F. Lim, Y.C. Liang, A. Suwardi, Appl. Phys. Lett. 103 (2013) 062901.
[32] J. Xie, C. Guo, P. Yang, X. Wang, D. Liu, C.M. Li, Nano Energy 31 (2017) 28–36.
[33] S. Li, B. AlOtaibi, W. Huang, Z. Mi, N. Serpone, R. Nechache, F. Rosei, Small 11 (2015) 4018–4026.
[34] Y. Li, J.Z. Zhang, Laser Photonics Rev. 4 (2010) 517–528.
[35] Y. Zhao, N. Hoivik, K. Wang, Nano Energy 30 (2016) 728–744.
[36] S.K. Karuturi, C. Cheng, L. Liu, L. Tat Su, H.J. Fan, A.I.Y. Tok, Nano Energy 1 (2012) 322–327.
[37] K. Peng, X. Wang, S.-T. Lee, Appl. Phys. Lett. 92 (2008) 163103.
[38] G. Wang, H. Wang, Y. Ling, Y. Tang, X. Yang, R.C. Fitzmorris, C. Wang, J.Z. Zhang, Y. Li, Nano Lett. 11 (2011) 3026–3033.
[39] S. Li, J. Zhang, M.G. Kibria, Z. Mi, M. Chaker, D. Ma, R. Nechache, F. Rosei, Chem. Commun. 49 (2013) 5856–5858.
[40] L. Gao, Y. Cui, J. Wang, A. Cavalli, A. Standing, T.T.T. Vu, M.A. Verheijen, J.E.M. Haverkort, E.P.A.M. Bakkers, P.H.L. Notten, Nano Lett. 14 (2014) 3715–3719.
[41] Y.-L. Huang, W.S. Chang, C.N. Van, H.-J. Liu, K.-A. Tsai, J.-W. Chen, H.-H. Kuo, W.-Y. Tzeng, Y.-C. Chen, C.-L. Wu, C.-W. Luo, Y.-J. Hsu, Y.-H. Chu, Nanoscale 8 (2016) 15795–15801.
[42] Y. Inoue, K. Sato, K. Sato, H. Miyama, J. Phys. Chem. 90 (1986) 2809–2810.
[43] W. Cui, Z. Xia, S. Wu, F. Chen, Y. Li, B. Sun, ACS Appl. Mater. Inter. 7 (2015) 25601–25607.
[44] W. Yang, Y. Yu, M.B. Starr, X. Yin, Z. Li, A. Kvit, S. Wang, P. Zhao, X. Wang, Nano Lett. 15 (2015) 7574–7580.
[45] Q.-P. Ding, Y.-P. Yuan, X. Xiong, R.-P. Li, H.-B. Huang, Z.-S. Li, T. Yu, Z.-G. Zou, S.-G. Yang, J. Phys. Chem. C 112 (2008) 18846–18848.
[46] J. Choi, S.Y. Ryu, W. Balcerski, T.K. Lee, M.R. Hoffmann, J. Mater. Chem. 18 (2008) 2371–2378.
[47] T. Zhang, K. Zhao, J. Yu, J. Jin, Y. Qi, H. Li, X. Hou, G. Liu, Nanoscale 5 (2013) 8375–8383.
[48] L. Yan, J. Zhang, X. Zhou, X. Wu, J. Lan, Y. Wang, G. Liu, J. Yu, L. Zhi, Int. J. Hydrogen Energy 38 (2013) 3554–3561.
[49] J. Lan, X. Zhou, G. Liu, J. Yu, J. Zhang, L. Zhi, G. Nie, Nanoscale 3 (2011) 5161–5167.
[50] T. Zhang, W. Lei, P. Liu, J.A. Rodriguez, J. Yu, Y. Qi, G. Liu, M. Liu, Chem. Sci. 6 (2015) 4118–4123.
[51] T. Zhang, W. Lei, P. Liu, J.A. Rodriguez, J. Yu, Y. Qi, G. Liu, M. Liu, J. Phys. Chem. C 120 (2016) 2777–2786.
[52] M. Khraisheh, A. Khazndar, M.A. Al-Ghouti, Int. J. Energ. Res. 39 (2015) 1142–1152.
[53] S. Park, C.W. Lee, M.-G. Kang, S. Kim, H.J. Kim, J.E. Kwon, S.Y. Park, C.-Y. Kang, K.S. Hong, K.T. Nam, Phys. Chem. Chem. Phys. 16 (2014) 10408–10413.
[54] S. Kim, J.-H. Lee, J. Lee, S.-W. Kim, M.H. Kim, S. Park, H. Chung, Y.-I. Kim, W. Kim, J. Am. Chem. Soc. 135 (2013) 6–9.
[55] P.G. Kang, T.K. Lee, C.W. Ahn, I.W. Kim, H.H. Lee, S.B. Choi, K.D. Sung, J.H. Jung, Nano Energy 17 (2015) 261–268.
[56] G.K.L. Goh, C.G. Levi, J. Hwan Choi, F.F. Lange, J. Cryst. Growth 286 (2006) 457–464.
[57] S. Nah, Y.-H. Kuo, F. Chen, J. Park, R. Sinclair, A.M. Lindenberg, Nano Lett. 14 (2014) 4322–4327.
[58] I.I. Naumov, H. Fu, Phys. Rev. Lett. 95 (2005) 247602.
[59] G. Lee, Y.-H. Shin, J.Y. Son, J. Am. Chem. Soc. 95 (2012) 2773–2776.
[60] A.Z. Simões, A. Ries, C.S. Riccardia, A.H. Gonzaleza, M.A. Zaghetea, B.D. Stojanovicb, M. Cilensea, J.A. Varelaa, Mater. Lett. 58 (2004) 2537–2540.
[61] P. Kubelka, F. Munk, Z. Tech. Phys. 12 (1931) 593–603.
[62] C. Liu, J. Sun, J. Tang, P. Yang, Nano Lett. 12 (2012) 5407–5411.
[63] G. Wang, H. Chen, Y. Li, A. Kuang, H. Yuan, G. Wu, Phys. Chem. Chem. Phys. 17 (2015) 28743–28753.

Shun Li received his B.E. Degree from Tianjin University in 2007, and his M.E. Degree from University of Science and Technology Beijing in 2010. He received his Ph.D. Degree in Energy and Materials Science from Institut national de la recherche scientifique (INRS), Canada in 2015. His research interests include nanomaterials and thin films for solar energy conversion.

Jianming Zhang is a professor at the School of Chemistry and Chemical Engineering of Jiangsu University. He received his Ph.D. degree in 2013 from Institut national de la recherche scientifique (INRS) in Canada. His research interests focus on photo-responsive nanomaterials for green chemistry processes and functional polymers.

Bo-ping Zhang is a professor of School of Materials Science and Engineering, University of Science and Technology Beijing, China. She received master and doctor degrees both from Tohoku University (Japan) in 1990 and 1993, and a bachelor degree from the Huazhong University of Science and Technology, China, in 1984. Before joining University of Science and Technology Beijing as a full professor in 2003, she worked in Tohoku University as a research fellow and lecturer from 1993 to 2003. Her current research interests include thermoelectric, piezoelectric and photocatalytic materials.

Wei Huang received his Master Degree in Materials for Structure and Energy from University of Paris-Sud 11 (France) in 2011. Then, he worked at the field of New Energy & Clean Technology in Beijing (China) in 2012. He is currently a Ph.D. student at Institut national de la recherche scientifique (INRS) in Canada. His research mainly focuses on all-inorganic multiferroic oxides thin film based devices such as photovoltaics and switchable photodiodes.

Catalin Harnagea (B.Sc. Physics, 1996) obtained his Ph.D. degree (2001) from Martin Luther University of Halle, Germany. He continued to study the patterning and ferroelectric properties of nanostructures at Max-Planck-Institut fuer Mikrostrukturphysik (Halle). Since 2003 he moved to National Institute for Scientific Research (Varennes, QC, Canada), where he diversified his research interests, which now include scanning probe microscopy applied to the study of (multi-)functional properties of nanostructures of semiconductors, simple/complex oxides, biomaterials with potential applications in energy and health sectors. Several of his over 100 peer-reviewed publications, had a significant impact on the understanding of the nanoscale electromechanical behavior of matter, particularly of nanostructures.

Riad Nechache (Ph.D. in Materials science and Engineering in 2009; Group leader at ÉTS since 2015). He is an international pioneer in the development of high-performance photovoltaic cells using multiferroic perovskite oxides and the first demonstrating the experimental synthesis of multiferroic Bi_2FeCrO_6 oxide by laser ablation process. His research experience is documented by more than 50 articles in prestigious international journals, including, Nature photonics, Advanced Materials, etc. He was awarded both the prestigious NSERC and FQRNT fellowships in 2011. His experience in projects related to perovskite oxides materials is outstanding, as evidenced by his published works becoming references for various groups over the world.

Lifeng Zhu received his Ph.D. degree from University of Science and Technology Beijing in 2015. He is working as a postdoctoral fellow in University of Science and Technology Beijing. His research focuses on high-performance lead-free piezoelectric materials.

Suwei Zhang received her Master and Ph.D. degree from University of Science and Technology Beijing in 2010 and 2017. Currently, she is working as a postdoctoral fellow in Tsinghua University. Her research focuses on photocatalysis, energy storage and piezoelectricity.

Yuan-Hua Lin is Changjiang Scholar Distinguished Professor of Materials Science at the School of Materials Science and Engineering, Tsinghua University. He received his BS degree from the East China Institute of Technology, his MS degree from the Institute of Process and Engineering, Chinese Academy of Sciences, and his Ph.D. degree from Tsinghua University. He was a scholar for the Japan Society for the Promotion of Science at the University of Tokyo in 2005. His main research interests include high-κ ceramics and thin films for high energy density capacitors applications; oxide-based diluted magnetic semiconductor thin films; and high-temperature oxide thermoelectric materials and devices for energy conversion. He has over 200 publications and 10 patents in these areas.

Liang Ni is a professor of School of Chemistry and Chemical Engineering of Jiangsu University. His research interest mainly focuses on the physical chemistry, interfacial catalysis and coordination chemistry.

Yuanhua Sang obtained his B.S. degrees at Shandong University in China in 2007 and completed his Ph.D. with Prof. Hong Liu at Shandong University in July 2012. Now, he works as a lecturer in State Key Laboratory of Crystal Materials, Shandong University, China. His research interests are structure and property investigation of inorganic crystal materials with neutron and X-ray diffraction, functional materials, and materials for solar light conversion.

Hong Liu is a professor in State Key Laboratory of Crystal Materials, Shandong University, and adjunct professor in Beijing Institute of Nanoenergy and Nanosystems, Chinese Academy of Science. He received his Ph.D. degree in 2001 from Shandong University. He has published over 200 refereed papers, and over 30 patents. In 2009, he received a Distinguished Young Scholar Award by the National Natural Science Foundation of China. In 2012, he was awarded the One Hundred Talents Professorship of CAS at Beijing Institute of Nanoenergy and Nanosystems. His current research focuses mainly on nonlinear crystal growth, chemical processing of nanomaterials for energy related applications including photocatalysis, energy storage and conversion, tissue engineering, especially the interaction between stem cell and nanostrucuture of biomaterials.

Federico Rosei is Professor and Director of the INRS Centre Énergie, Matériaux et Télécommunications, Varennes (QC) Canada. He holds the UNESCO Chair in Materials and Technologies for Energy Conversion, Saving and Storage and the Senior Canada Research Chair in Nanostructured Materials. He received MSc and Ph.D. degrees from the University of Rome "La Sapienza" in 1996 and 2001, respectively. He has received several awards and is Fellow/Member of many prestigious societies and academies, including the Royal Society of Canada, the European Academy of Sciences, the American Physical Society, the World Academy of Arts and Science, the Chinese Chemical Society (Honorary), the American Association for the Advancement of Science, SPIE, the Canadian Academy of Engineering, ASM International and the Engineering Institute of Canada.